Optimization of Microchannel Heat Sink for Thermal Performance and Pressure Drop using Central Composite Design of Experiment

Mohamad Nur Hidayat Mat
Faculty of Mechanical Engineering, Universiti Teknologi Malaysia

Normah Mohd-Ghazali
Faculty of Mechanical Engineering, Universiti Teknologi Malaysia

Hielfarith Suffri Shamsuddin
Faculty of Mechanical Engineering, Universiti Teknologi Malaysia

Patrice Patrice Estellé
Univ Rennes, LGCGM

https://doi.org/10.5109/7183463

出版情報：Evergreen. 11 (2), pp.1426-1434, 2024-06. 九州大学グリーンテクノロジー研究教育センター
バージョン：

Optimization of Microchannel Heat Sink for Thermal Performance and Pressure Drop using Central Composite Design of Experiment

Mohamad Nur Hidayat Mat[1, *], Normah Mohd-Ghazali[1], Hielfarith Suffri Shamsuddin[1], Patrice Patrice Estellé[2]

[1]Faculty of Mechanical Engineering, Universiti Teknologi Malaysia, 81310 UTM Johor Bahru, Malaysia

[2]Univ Rennes, LGCGM, F-35000 Rennes, France

*Author to whom correspondence should be addressed:
E-mail: mn.hidayat@utm.my

(Received June 15, 2022; Revised March 11, 2024; Accepted June 14, 2024).

Abstract: By using an analytical optimization approach on a rectangular microchannel heat sink, this research aims to increase thermal efficiency and decrease pressure drop.By using a central composite design, the experimental setup maintains a consistent volume flow rate of 4.6 cm3/s for the water coolant. In advance of numerical study, a single symmetrical microchannel heat sink was segmented using computational fluid dynamics (CFD). In consideration of several goals, 2500 design points were developed using a response surface method-based optimization technique (RSM). The genetic algorithm used for elitist non-dominated sorting was utilised to ascertain the optimal design points in compliance with the given criteria (NSGA2). The agreement between the outcomes of the model and the current inquiry was verified by means of validation using previous experimental data. The research results indicate that as compared to the base design, there is a significant decrease of 53.29 percent in pressure drop and a potential gain of 17.27 percent in thermal performance. This improvement was achieved with the adjustment of the wall width ratio to 0.0014 and the channel aspect ratio to 1.11. The increased temperature difference may be attributed to the increased surface area contact between the silicone and the fluid, which is achieved by using 143 channels instead of 100 channels in the prior model. The use of this approach results in progress in the development of microchannel heatsinks, particularly those utilised with water-based coolants. As a result, the power consumption of the pump is decreased and the rate of heat dissipation from limited areas is accelerated.

Keywords: CFD; microchannel heat sink; nanofluid; optimization; surfactant

1. Introduction

The advent of the fourth industrial revolution has prompted a global transition from conventional manufacturing methods to comprehensive automated systems. Consequently, there is a growing need to optimize system efficiency to support increased production outputs and extended operational durations. This circumstance has allowed 3-6 billion integrated transistors, resistors, and other micro components to be installed in a single electrical chip. This has caused the biggest concern by industry on excess heat generated from this component as it was reported that approximately 30% of the product's damage due to improper heat sink management system [citation]. Due to this damage, some industries may bear the cost and rejected products that outrageously damage the company profit and income generation. Therefore, it is crucial to efficiently get rid of excessive heat flux generation from heavy electrical devices. Additionally, a microchannel heatsink (MCHS) shows potential as an effective method for dispersing significant heat generated in a confined space. The MCHS functions as a compact and passive heat exchanger on a micron scale, efficiently transferring heat from electronic or mechanical devices to a cooling fluid medium. This heatsink has placed a great focus by researchers in recent years in improving the system design by analyzing its characteristic and behavior toward thermal performance and pressure drop. Many studies have suggested that the key to achieving better system performance by lowering thermal resistance and minimizing pressure drop across microchannel heatsink channel simultaneously. This would improve the system performance in terms of long operation hours due to quick heat dissipation and reducing

power consumption because of lower pressure drop [1]. The recent investigation into microchannel heat sinks (MCHS) has prompted researchers to explore alternative methods for enhancing their capabilities through the use of different structural materials. Various approaches have been employed, including the utilization of different cooling fluids, alternative rib channels, channel porosity adjustments, and exploration of different channel geometries [1].

Heat transmission and fluid motion in microchannels have been the subject of much academic investigation. An examination was undertaken by Sobhan and Garimella [2] to examine the heat transmission and fluid motion phenomena that take place inside microchannels. Toh and Chen performed analysis of friction factor along the channel against the local heat transfer coefficient inside microchannel heat sink. The Navier-Stokes equations were solved in three dimensions, taking into account the temperature-dependent flow behaviour [3]. In order to investigate the thermal dynamics and fluid motion inside microchannels, however, classic Navier–Stokes equations [4–7] may prove outdated.

Microsystem scaling effects were proposed by Herwig and Hausner [8]. While Xu and Ooi [9] looked into microchannel liquid flow, another group studied the effect of viscous dissipation. Reduced velocity gradients in smaller hydraulic channels were highlighted as an important factor to consider. The effect of viscous dissipation on temperature and friction variables in circular and rectangular microchannels was studied by Koo and Kleinstreuer. The researchers found an interesting relationship between the hydraulic system's diameter and the channel's aspect ratio [10,11].

Heat transmission and fluid flow in microchannels have been the subject of several empirical experiments by a large group of researchers. Their research indicates that our understanding of the mechanisms controlling heat transfer and pressure reduction is still quite intact [11]. It was Nunes and Cotta who studied forced convection systems with a single phase [12]. However, the importance of temperature-dependent properties in heat transfer was further highlighted by Herwig and Mahulikar [13] due to the scaling effects of Reynolds number and axial temperature gradient.

Li and Huai conducted numerical investigations to analyse laminar flow inside rectangular microchannels for the purpose of heat and water transfer. They advocated for the use of the variable property method in engineering applications, emphasising its capacity to capture observable events with precision [14]. The inclusion of viscous dissipation and thermophysical parameters in microchannel heat transfer calculations is indisputable [15-18]

In addition, many computational and analytical methods, including fin models, have been used to improve the microchannel morphology [19–24]. Regardless, there is a dearth of literature on optimised full-model microchannels [25], which include the whole fluid flow and concomitant heat transfer process. When designing fin models for rectangular microchannel heat sinks with large aspect ratios, Kim (25) proposed an optimization method to overcome the problems caused by the assumptions used. In an attempt to improve design models, Li and Peterson [26] used solid and fluid analysis to study the parametric form of rectangular microchannels. Husain and Kim [27] used numerical methods and a surrogate technique to enhance the geometric features of microchannels operating at a constant pumping power.

To optimise microchannel heat sinks, analytical and numerical studies were effectively combined with evolutionary algorithms, namely the elitist non-dominated sorting genetic algorithm [28]. (NSGA-II). The current research is focused on improving microchannel heat sinks' thermal resistance and pumping capacity using a multi-objective framework. Additional experimental designs for central composites might benefit from this method's use [28]. It is possible to speed up the search for optimal solutions for evolutionary algorithms by setting objective function values and then using the response surface approach together.

2. Methodology

2.1 Physical model and boundary condition

The dimensions of the microchannel heat sink's channels are 10 mm by 10 mm by 0.213 mm, as seen in Fig. 1. (length x width x substrate thickness). Each channel inside this silicon-based structure is symmetrical over its entire length. In order to reduce computational load and streamline processes, a certain symmetrical portion of the channel was chosen as the computational domain. Utilizing computation-aided design (CAD), the geometric representation of this numerical domain was produced. The basic equations necessary for calculations in the numerical realm include the principles of momentum, energy, and mass conservation [29]. One of the aspects that they especially address is convective heat transmission inside the microchannel. The following section provides an illustration of how these equations may be expressed in tensor form.

Conservation of Mass:

$$\frac{\partial \rho_f}{\partial t} + \frac{\partial \rho_f u_i}{\partial x_i} = 0 \quad (1)$$

Conservation of Momentum:

$$\rho_f \frac{\partial u_i}{\partial t} + \rho_f \frac{\partial u_i}{\partial x_j} = -\frac{\partial p}{\partial x_i} + \rho_f g_i + \frac{\partial}{\partial x_j}\left(\mu_f \frac{\partial u_i}{\partial x_j}\right) + \frac{\partial}{\partial x_j}\left(\mu_f \frac{\partial u_j}{\partial x_i}\right) - \frac{2}{3}\frac{\partial}{\partial x_j}\left(\mu_f \frac{\partial u_k}{\partial x_k}\right) = 0 \quad (2)$$

Conservation of Energy:

$$\rho_f \frac{\partial h}{\partial t} + \rho_f u_j \frac{\partial h}{\partial x_i} = \frac{\partial p}{\partial t} + u_i \frac{\partial p}{\partial x_i} + \frac{\partial}{\partial x_i}\left(k_f \frac{\partial T_f}{\partial x_i}\right) + \tau_{ij}\frac{\partial u_i}{\partial x_j} \quad (3)$$

(For fluid domain)

$$\frac{\partial}{\partial x_i}\left(k_s \frac{\partial T_s}{\partial x_i}\right) = 0 \quad \text{(For substrate conduction)} \quad (4)$$

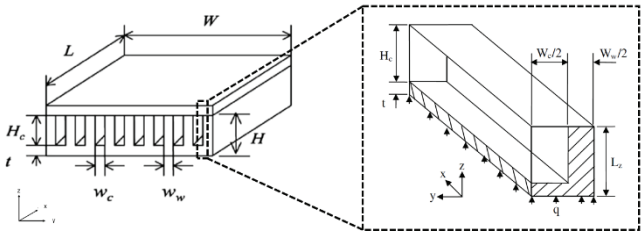

Fig. 1: Schematic drawing of simplified microchannel

As seen in Table 1, the mathematical representation requires the repeated resolution of boundary conditions at each cell centroid. Regarding the lower surface area of the heat sink, 790 W/cm2 of uniform heat flow was implemented. The prevailing assumption was that convective heat transfer and radiation ensured that the bulk of outside surfaces remained completely insulated from the environment. By imposing symmetrical boundary constraints on the heat sink planes' x and z coordinates. The volumetric flow rate and temperature of the fluid were determined to be 4.7 cm3/s and 23°C, respectively, at the inlets of the heat sink. In contrast, a constant static pressure was maintained at the outflow of the channel. When the energy equations of the fluid and wall were integrated, the conjugate boundary condition was the continuity of temperature and heat flow. The numerical solutions of Equations (1) through (4) were obtained by the use of an Ansys Fluent solver designed for finite volume computational fluid dynamics (CFD) [1].

Table 1. Setup boundary condition.

Boundary condition	Value	Source
Analysis type	Steady state	[30]
Type of flow	Laminar	[30]
Number of cycles	400	[30]
Ambient temperature	23℃	[31]
Inlet flux	4.7 cm^3/s	[31]
Outlet flux	0 Pa	[31]
Heat flux	790 W/cm^2	[32]
Pressure correction type	SIMPLE	[30]
Mass convergence criteria	$1x10^4$	[27]
velocity convergence criteria	$1x10^4$	[27]
Energy convergence criteria	$1x10^7$	[27]

2.2 Mesh sensitivity study and validation

In this investigation, fluid flow across the channel was simulated with structured meshes. On the walls, however, a little improvement in the form of a growth rate of 1.2 was incorporated. The respective convergence requirements for energy, mass, and velocity were established at 1x107, 1x104, and 1x104 [1]. The connection of pressure and velocity was accomplished with the SIMPLE method. In order to faithfully represent the boundary conditions and viscous shear layer, the process of mesh refinement was concentrated on the interfaces between the solid and liquid phases. A minimum mesh size of 0.005 mm was utilised for this purpose. The purpose of doing a sensitivity analysis of mesh density was to ensure the most accurate representation of infinitesimally small mesh dimensions [2–4]. The mesh size used is a critical factor in computational fluid dynamics (CFD) when it comes to attaining experimental value matching [5–7].

As seen in Fig. 3, three distinct kinds of meshes—coarse, medium, and fine—were created and visually represented. One characteristic of each mesh type is a typical cell length. Although reduced mesh sizes offer enhanced precision, they impose excessive computing requirements, which makes them impracticable for comprehensive analyses. As a result, thermal resistance values corresponding to microscopic mesh sizes were estimated by extrapolation. The relative errors were subsequently computed with the fine mesh serving as a reference and under these ideal conditions. As detailed in Table 2, the iterative procedure for producing mesh types was repeated until relative errors fell below 5 percent.

Table 2. Comparison of the current results and Tuckerman & Pease's results.

α	β	Tuckerman & Pease	Present simulation	Error (%)
		Pumping power (W)		
5.710	0.780	0.486	0.508	4.53
6.010	1.000	1.838	1.912	4.03
5.218	0.818	0.762	0.795	4.33

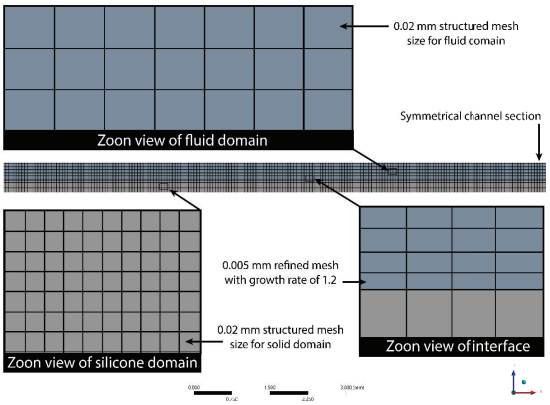

Fig. 2: Mesh refinement near interface layer.

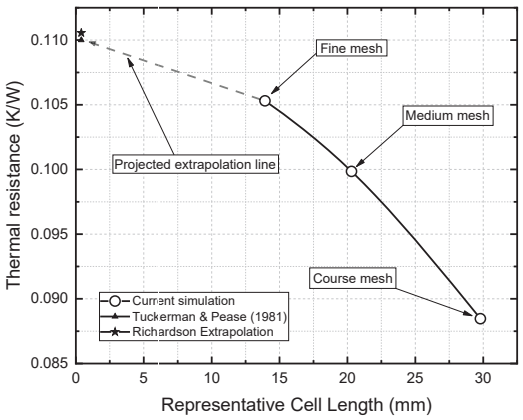

Fig. 3: Mesh sensitivity plot.

2.3 Optimization Method

Utilizing a four-level factorial design methodology, the researchers selected two optimization variable parameters denoted as (Hc/Wc) and (Ww/Wc). The limits of the design variable are summarised in the table that follows. In order to ascertain the relationship between thermal resistance, pumping power, and microchannel and fin width, the optimization approach ensured that the microchannel depth (Hc) remained constant. By using two distinct target functions, this research enhances a microchannel heat sink by decreasing both thermal resistance and pumping power consumption.

Table 3. Design variable and constrain.

Design variables	Lower limit	Upper limit
α	5	1
β	0.01	0.1
Heat sink width, W (cm)	1	
Heat sink length, L (cm)	1	
Substrate thickness, t (cm)	0.0213	
Channel height, H_c (cm)	0.032	

The heat transfer efficiency is defined by the pumping power and thermal resistance required to move the coolant through the microchannel. What follows is an explanation of total thermal resistance.

$$R_{th} = \frac{\Delta T_{max}}{q A_s} \quad (5)$$

ΔT_{max} is the greatest increase in heat sink temperature, while A_s is the area of the heat flux substratum

$$\Delta T_{max} = T_{s,o} - T_{f,i} \quad (6)$$

Finding out how much pumping power is needed to transfer the fluid through the sink is doable.

$$\bar{P} = n \cdot u_{avg} \cdot A_c \cdot \Delta p \quad (7)$$

Δp represented by pressure drop, and u_{avg} is the average velocity of fluid flow.

2.3 Multi-Objective Genetic Algorithm

The current matter pertains to two contradictory objectives, in which advancements towards one consequence result in the deterioration of the other. The procedures utilised in order to determine the optimal global Pareto front are depicted in Fig. 4. The numerical evaluation and theoretical description of the objective functions are performed. An evolutionary strategy that combines many objectives is utilised to provide optimum global Pareto solutions. In the beginning, approximate optimum solutions for two objective functions are constructed utilising coded NSGA-II, which incorporates real space crossover and mutation operations. Following this, the solutions are refined through the process of determining the optimal local solution for every objective function across the whole NSGA-II. Once the first solution estimate is completed using NSGA-II sequential quadratic programming (SQP), two distinct local search algorithms are used. Using a composite target and optimal search, all objectives may be optimised in one place, but only if optimising one goal makes optimising the others necessary. When it comes to optimising for many objectives at once, this method is a huge step forward in the optimization field. The technique efficiently reduces the time required to find optimum solutions by prioritising the optimization of the major aim and discarding limitations on equality. This technique is significantly more effective when it uses NSGA-capability II's to address problems with multi-objective optimization. Removing dominated and duplicate solutions allows us to concentrate on the most promising Pareto optimum frontier alternatives. The solution space may be explored more thoroughly with the help of this method. By allowing the discovery of representative solutions that provide considerable insights into the given problem, local search increases the quality of the solutions.

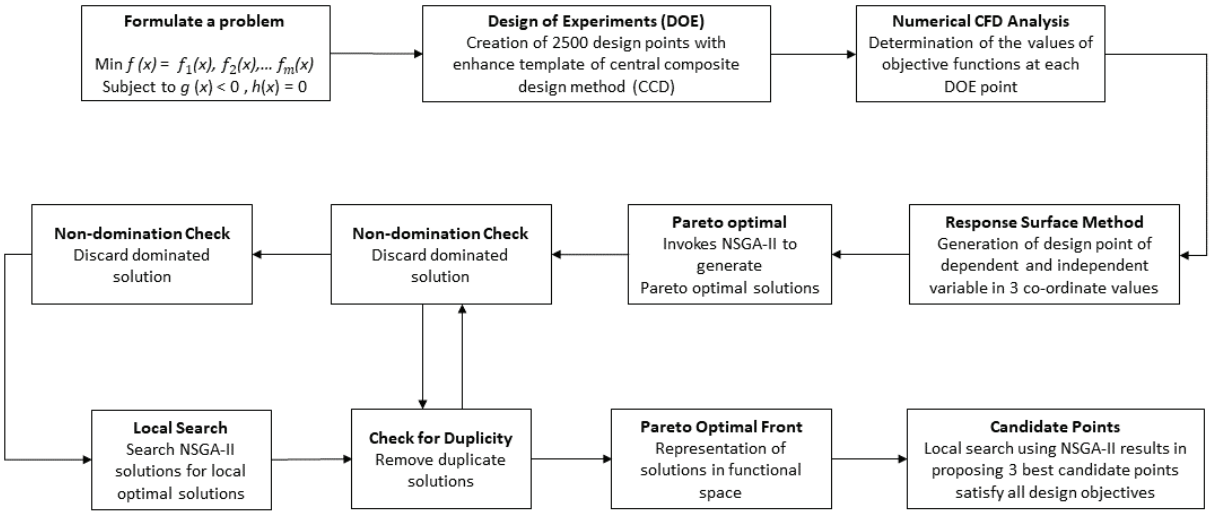

Fig. 4: Multi-objective optimization procedure.

3. Result and Discussion

3.1 Contour Plot Analysis

Results for thermal resistance and pumping power with respect to several independent factors are shown in Fig. 5 as contour plots. The relationship between the thermal resistance, the channel's aspect ratio (i), and the wall's width ratio (a) is shown in Fig. 5a. Both a rise and a reduction in i have resulted in a decrease in the thermal resistance. According to a prior study by Halelfadl and Adham [31], this association is in line with their findings. They found that when a (H_c/W_c) expanded, channel dimensions decreased and wall dimensions contracted, leading to an increase in the number of channels per system. There is a greater contact surface area between the liquid and fluid areas when the number of channels is increased. On the contrary, the correlation between i and a and pumping power is seen in Fig. 5b. Generally, a reduction in both i and a leads to a decrease in the amount of pumping force needed. This correlation was corroborated in a prior investigation conducted by Qu and Mudawar [39], which demonstrated that a reduction in the values of both parameters leads to an enlargement of the channel and a contraction of the wall. The velocity flow is influenced by the channel size, with a larger cross-sectional area resulting in a lower fluid pressure. The influence of the Reynolds number (Re) and heat resistance is seen in Fig. 5c. Enhancing thermal performance by substantially decreasing thermal resistance originating from the flow property in the context of laminar flow. This is possible by the enlargement of a channel. According to the continuity equation [40], velocity and cross-sectional area are correlated. In addition, Re are illustrated in relation to pumping power in Fig. 5d. In general, a decrease in i that leads to a reduction in Re would diminish the amount of energy needed to pump the fluid through the channels. Furthermore, the value of Re is impacted by the values of i and a. This would have an impact on the medium flow that traverses the canal. Hence, to optimise heat transfer efficiency between the fluid medium and the wall, it is necessary to decrease the flow rate, hence providing enough time for heat to dissipate from the heat source [41]. A visually attractive illustration of the association between the Reynolds number (Re), the fin parameter (ω), and thermal resistance in the Microchannel Heat Sink is shown in Fig. 5e (MCHS). The graph aptly illustrates that concurrent decreases in both Re and β are necessary to decrease thermal resistance, with the latter needing a minimum value of 0.05. This finding underscores the critical need of doing a comprehensive geometric analysis to determine the optimal design parameters that reduce thermal resistance in configurations that use MCHS.

Regarding Figure 5f, which explores the intricate relationship among β, Re, and pumping power demands, an intriguing finding comes to light. The lower spectrum of pumping power characteristics, as seen in the graph, comprises the values of 0.01 to 0.04 of the wall width ratio (β). This discovery is in opposition to the expected pattern found in thermal resistance, in which an increase in β is often associated with increased pumping power demands. Nevertheless, it is worth mentioning that this inconsistency remains intact just until a β value of 0.05 is exceeded; after that point, the predominant tendency is the reduction of heat resistance, even if this may result in an increase in pumping power requirement.

The aforementioned observations highlight the critical interplay of geometric factors, heat transfer efficiency, and flow dynamics in MCHS systems. They emphasise the criticality of developing a comprehensive comprehension of these correlations in order to optimise MCHS design for improved thermal management efficiency and reduced energy usage. Under the guidance of these insights, more study and experimentation have the potential to propel the development of thermal management systems that are more efficient and effective.

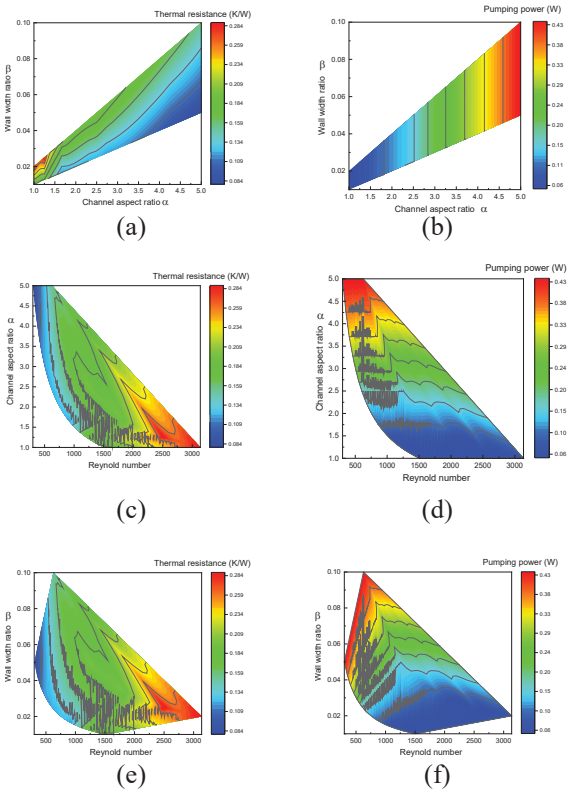

Fig. 5: Contour plot of design variables against objective function.

3.2 Comparison Based and Optimized Design

Comparison study of optimized and based design model by Tuckerman and Pease [32] is presented in Table 4. The value of channel aspect ratio, α and wall width ratio, β for optimum design are 1.11 and 0.014, respectively. Optimized design has improved based design by 17.27 % dropping in thermal resistance while more than half improved pumping power consumption. Figure 6 presents the comparison between the based design proposed by Tuckerman and Pease [32] with a current of optimized design. The values of interest were measured using relative length *(x/L)* on different relative height *(y/H_c)*. Figure 6a presents the relationship between relative length across a channel section with thermal resistance. Increasing *(x/L)*, decreases the value of thermal resistance; however, optimized design obviously shows dropping in thermal resistance as *(x/L)* away from the inlet. Figure 6b reveals the relationship of relative length with outlet temperature. This can be seen that outlet temperature for an optimum design higher than based design. In other words, optimum design dissipates more heat than the based design. The significant different obviously happens when the relative length away from the channel inlet. Figure 6c shows the relationship between pressure drop and relative length. Pressure drops directly proportional to pumping power. The overall trend has shown that optimum design has a lower pressure drop approximately around 7 psi while based on 15 psi. The highest pressure for both models occur at the inlet section and reduce to a minimum till the outlet section, as presented in the chart. Figure 6d, on the other hand demonstrates the correlation of Reynold number (*Re*) with relative length. The relative length shows for both models almost sideways trend across the channel length but start with minimum *Re* at the inlet section. Optimized design shows significant flow type as compared to based design as optimized design flow completely laminar flow as the value is less than 1500 for a rectangular channel.

Table 4. Comparison of optimization with based design.

Design parameter	**Optimum design**	**Based design [32]**
α	1.11	5.71
β	0.014	0.78
Thermal resistance, R, (K/W)	0.091	0.11
Pumping power, P_p	0.227	0.486
$\Delta R/R$ (%)	17.27 (Improved thermal performance)	
$\Delta P_p/ P_p$ (%)	53.29 (Lower pumping power requirement)	

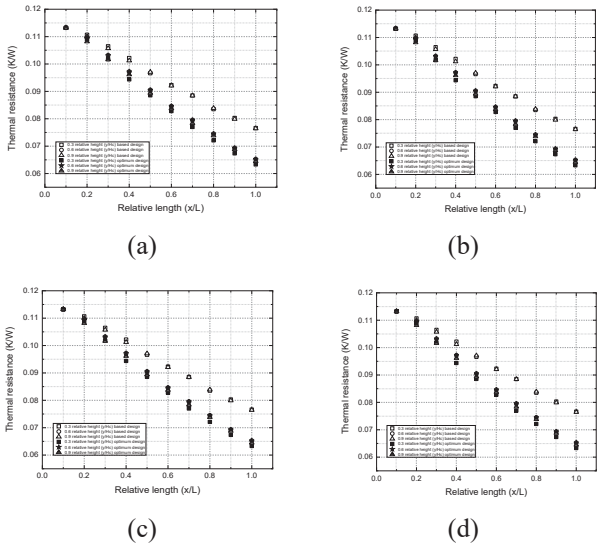

Fig. 6: Comparison of based design with optimized model.

3.3 Flow pattern along channel

Contour plot view for total pressure, temperature, and velocity magnitude with two different cross-sectional views in the x and y plane shown in Fig. 7and Fig. 8, respectively. The sum of the flow's static and dynamic pressures is shown by the total pressure contour map. Figure 7 shows that compared to the basic design, which has a high initial pressure of around 120 kPa, the optimal

design contour plot starts out with a low pressure of about 60 kPa. The optimal design results in about half the pressure drops of the based design, it follows. Put another way, the optimal design uses half as much pumping power as the basic design model.Furthermore, additional cross-sectional views can be seen from Fig. 8 under total pressure at different relative lengths, x/L = 0, 0.5, and 1. These three different relative lengths represent the inlet, middle and outlet view. Figure 7 for temperature contour plot on the other hand, optimum design, especially at the outlet section, dissipate more heat around 60 ℃ than the based design. When the outlet section is viewed in x-plane, temperature distribution evenly happens at the outlet section compared to the based design. It seems the based design showing incomplete dissipation of heat transfer from solid to fluid medium. Velocity magnitudes play an important role in making sure the flow under completely laminar to transient state flow. For optimum design, the average flow around two m/s while based design roughly around four m/s. The flow has different velocity. However, the mass flow rate still constant throughout the analysis. This is due to the geometrical change of both designs model.

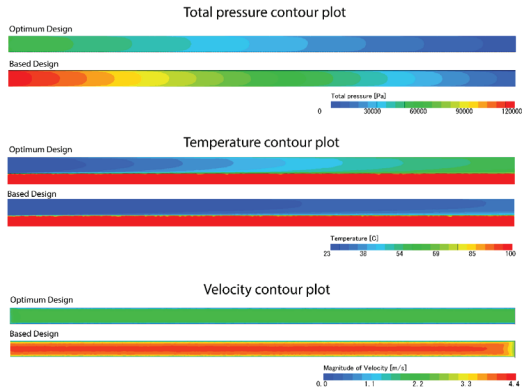

Fig. 7: Contour plot of cross section y-plane view

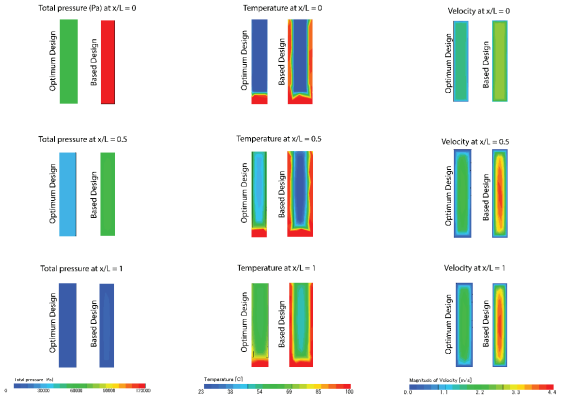

Fig. 8: Contour plot of cross section x-plane view between optimized and based design.

4. Conclusion

This work used an optimization inquiry using a central composite design of experiment to find the places with the lowest local thermal resistance and pumping power, and then an elitist non-dominated sorting genetic algorithm (NSGA2) to choose the places that met all the design requirements.Therefore, the research has successfully achieved its objective via the determination of optimum design parameters that maximise heat energy dissipation and minimise pressure drop. After conducting an examination, it was found that:

- In the ideal design, the values of α (channel aspect ratio) and β (wall width ratio) are 1.11 and 0.014, respectively.
- The optimized design has improved based design by 17.27 %, dropping in thermal resistance.
- The optimum design requires half pumping power consumption around 53.29 % than the based design model.
- Thermal resistance is indirectly proportional to pumping power requirement and increasing α and reducing β results in reducing thermal resistance.
- Improving thermal performance by reducing thermal resistance can be done by controlling fluid flow and increasing the size of a channel.

Acknowledgements

The authors would like to acknowledge Universiti Teknologi Malaysia (UTM) for providing CFD facility in conducting this research project.

Nomenclature

CFD	computational fluid dynamics
MCHS	Microchannel heat sink
NSGA	Non-dominated sorting genetic algorithm
ρ	density (kgm^{-3})
u	flow velocity (ms^{-1})
T	temperature (K)
α	Channel aspect ratio
β	wall width ratio
R	thermal resistance (K/W)
P_p	pumping power (W)

References

1) Olabi, A., et al., *Application of nanofluids for enhanced waste heat recovery: a review.* Nano Energy, 2021: p. 105871.

2) Sobhan, C.B. and S.V. Garimella, *A comparative analysis of studies on heat transfer and fluid flow in microchannels.* Microscale Thermophysical Engineering, 2001. 5(4): p. 293-311.
3) Toh, K., X. Chen, and J. Chai, *Numerical computation of fluid flow and heat transfer in microchannels.* International Journal of Heat and Mass Transfer, 2002. 45(26): p. 5133-5141.
4) Cha, J., J. Seo, and S. Kim, *Building materials thermal conductivity measurement and correlation with heat flow meter, laser flash analysis and TCi.* Journal of thermal analysis and calorimetry, 2012. 109(1): p. 295-300.
5) Abro, K.A., et al., *Dual thermal analysis of magnetohydrodynamic flow of nanofluids via modern approaches of Caputo–Fabrizio and Atangana–Baleanu fractional derivatives embedded in porous medium.* Journal of Thermal Analysis and Calorimetry, 2019. 135(4): p. 2197-2207.
6) Safaei, M.R., et al., *Thermal analysis of a binary base fluid in pool boiling system of glycol–water alumina nano-suspension.* Journal of Thermal Analysis and Calorimetry, 2021. 143(3): p. 2453-2462.
7) Amjad, M., et al., *Thermal analysis of Casson micropolar nanofluid flow over a permeable curved stretching surface under the stagnation region.* Journal of Thermal Analysis and Calorimetry, 2021. 143(3): p. 2485-2497.
8) Herwig, H. and O. Hausner, *Critical view on "new results in micro-fluid mechanics": an example.* International Journal of Heat and Mass Transfer, 2003. 46(5): p. 935-937.
9) Xu, B., et al., *Evaluation of viscous dissipation in liquid flow in microchannels.* Journal of micromechanics and microengineering, 2002. 13(1): p. 53.
10) Koo, J. and C. Kleinstreuer, *Viscous dissipation effects in microtubes and microchannels.* International journal of heat and mass transfer, 2004. 47(14-16): p. 3159-3169.
11) Morini, G.L., *Single-phase convective heat transfer in microchannels: a review of experimental results.* International journal of thermal sciences, 2004. 43(7): p. 631-651.
12) Nunes, J., et al., *Conjugated heat transfer in microchannels*, in *Microfluidics Based Microsystems*. 2010, Springer. p. 61-82.
13) Herwig, H. and S.P. Mahulikar, *Variable property effects in single-phase incompressible flows through microchannels.* International journal of thermal sciences, 2006. 45(10): p. 977-981.
14) Li, Z., et al., *Effects of thermal property variations on the liquid flow and heat transfer in microchannel heat sinks.* Applied Thermal Engineering, 2007. 27(17-18): p. 2803-2814.
15) Rouf, R.A., et al., *Energy management and heat storage for solar adsorption cooling.* EVERGREEN Joint Journal of Novel Carbon Resource Sciences & Green Asia Strategy, 2016. 3(2): p. 1-10. doi.org/10.5109/1800866
16) Sultan, M., et al., *6: 3 EVERGREEN Joint Journal of Novel Carbon Resource Sciences & Green Asia Strategy, Vol. 01., Issue02, pp. 5-11 September 2014.* doi.org/10.5109/1495157
17) Li, C. and K. Ito, *Performance Evaluation of Wind Decontamination System by Computational Fluid Dynamics.* Evergreen: joint journal of Novel Carbon Resource Sciences & Green Asia Strategy, 2014. 1(2): p. 12-17. doi.org/10.5109/1495158
18) Mohd, N., et al., *Lattice boltzmann method for free surface impacting on vertical cylinder: A comparison with experimental data.* Evergreen: joint journal of Novel Carbon Resource Sciences & Green Asia Strategy, 2017. 4(2): p. 28-37. doi.org/10.5109/1929662
19) Knight, R.W., et al., *Heat sink optimization with application to microchannels.* IEEE Transactions on Components, Hybrids, and Manufacturing Technology, 1992. 15(5): p. 832-842.
20) Wei, X. and Y. Joshi, *Optimization study of stacked micro-channel heat sinks for micro-electronic cooling.* IEEE transactions on components and packaging technologies, 2003. 26(1): p. 55-61.
21) Fisher, T.S. and K.E. Torrance, *Optimal shapes of fully embedded channels for conjugate cooling.* IEEE Transactions on advanced packaging, 2001. 24(4): p. 555-562.
22) Weisberg, A., H.H. Bau, and J. Zemel, *Analysis of microchannels for integrated cooling.* International Journal of Heat and Mass Transfer, 1992. 35(10): p. 2465-2474.
23) Alhamid, M., et al., *Refrigeration cycle exergy-based analysis of hydrocarbon (r600a) refrigerant for optimization of household refrigerator.* Evergreen, 2019. 6(1): p. 71-77. doi.org/10.5109/2321015
24) Ardiansyah, S.R., et al., *Tubular photobioreactor: A preliminary experiment using synechococcus sp.(cyanobacteria) cultivated in NPK media for biomass production as biofuel feedstock.* Evergreen, 2019. 6(2): p. 157-161. doi.org/10.5109/2321011
25) Kim, S.J., *Methods for thermal optimization of microchannel heat sinks.* Heat transfer engineering, 2004. 25(1): p. 37-49.
26) Li, J. and G. Peterson, *Geometric optimization of a micro heat sink with liquid flow.* IEEE Transactions on Components and Packaging Technologies, 2006. 29(1): p. 145-154.
27) Husain, A. and K.-Y. Kim. *Design Optimization of Micro-Channel for Micro Electronic Cooling*. in *ASME 2007 5th International Conference on Nanochannels, Microchannels, and Minichannels*. 2007. American Society of Mechanical Engineers Digital Collection.

28) Foli, K., et al., *Optimization of micro heat exchanger: CFD, analytical approach and multi-objective evolutionary algorithms.* International Journal of Heat and Mass Transfer, 2006. 49(5-6): p. 1090-1099.
29) Taylor, M.A., *Conservation of mass and energy for the moist atmospheric primitive equations on unstructured grids*, in *Numerical techniques for global atmospheric models*. 2011, Springer. p. 357-380.
30) Hong, F., et al., *Conjugate heat transfer in fractal-shaped microchannel network heat sink for integrated microelectronic cooling application.* International Journal of Heat and Mass Transfer, 2007. 50(25-26): p. 4986-4998.
31) Halelfadl, S., et al., *Optimization of thermal performances and pressure drop of rectangular microchannel heat sink using aqueous carbon nanotubes based nanofluid.* Applied thermal engineering, 2014. 62(2): p. 492-499.
32) Tuckerman, D.B. and R.F.W. Pease, *High-performance heat sinking for VLSI.* IEEE Electron device letters, 1981. 2(5): p. 126-129.
33) Mat, M.N.H., et al., *Optimizing nozzle convergent angle using central composite design on the particle velocity and acoustic power level for single-hose dry ice blasting nozzle.* Journal of Thermal Analysis and Calorimetry, 2021. 144(6): p. 2159-2173.
34) Mat, M.N.H., et al., *Influence of nozzle area ratio on the gas-particle flow for single-hose dry ice blasting nozzle.* Journal of Thermal Analysis and Calorimetry, 2021. 143(3): p. 2343-2354.
35) Mat, M.N.H., et al., *Influence of divergent length on the gas-particle flow in dual hose dry ice blasting nozzle geometry.* Powder Technology, 2020. 364: p. 152-158.
36) Mat, M.N.H., et al., *Effect of impact force for dual-hose dry blasting nozzle geometry for various pressure and distance: an experimental work.* The European Physical Journal Plus, 2020. 135(2): p. 1-11.
37) Mat, M.N.H., et al., *Optimizing dry ice blasting nozzle divergent length using CFD for noise reduction.* CFD Letters, 2019. 11(6): p. 18-26.
38) Mat, M.N.H. and N. Asmuin, *Optimizing nozzle geometry of dry ice blasting using CFD for the reduction of noise emission.* International Journal of Integrated Engineering, 2018. 10(5).
39) Qu, W. and I. Mudawar, *Experimental and numerical study of pressure drop and heat transfer in a single-phase micro-channel heat sink.* International journal of heat and mass transfer, 2002. 45(12): p. 2549-2565.
40) Seis, C. *A quantitative theory for the continuity equation*. in *Annales de l'Institut Henri Poincaré C, Analyse non linéaire*. 2017. Elsevier.
41) Zhang, H., et al., *Thermal energy storage: Recent developments and practical aspects.* Progress in Energy and Combustion Science, 2016. 53: p. 1-40.
42) Leonard, B., *Alternative interpretations of the mole and the ideal gas equation.* Accreditation and quality assurance, 2011. 16(11): p. 577-581.
43) Bondareva, N.S. and M.A. Sheremet, *Flow and heat transfer evolution of PCM due to natural convection melting in a square cavity with a local heater.* International Journal of Mechanical Sciences, 2017. 134: p. 610-619.